On the design of a Magneto-Optical Kerr probe for measurements in High fields and at low temperatures.

Wilhelmus J. Geerts
National High Magnetic Field Laboratory
Tallahassee
Department of Materials Science
University of Florida, Gainesville.
Saturday, August 02, 1997

Abstract: A unique apparatus to measure the magneto-optical (MO) properties of ultra thin magnetic films and multilayers at high fields (20 Tesla) and low temperatures (2-325 Kelvin) was developed. The realized equipment has a sensitivity in the sub-mdegree range (10-8 10-9 emu for iron), and can be used to measure the MO properties in reflection and transmission mode. It has been added to the user accessible instruments at the NHMFL facilities in Tallahassee. Via this probe some new technologies, i.e. magnetic shielding, direct optics, and temperature control without exchange gas, were introduced to the magnet lab.
This reports discusses and describes the design of the probe. After some introductory chapters (motivation for a MO high field probe & overview high field facilities), the choice of the measurement technique will be clarified. The second part of the manuscript contains most of the “whys” and “why nots” of the first three prototypes (MOK1-3). Technical drawings and additional information can be found in the appendices.
A user manual of the equipment is available from Dr. Bruce Brandt, director of Operations, 1800 E. Paul Dirac Dr. Tallahassee.

Lack of sufficient time forced me to write the report in the 30/70 mode. Errors and/or ambiguities, will be there: I hope you learn from them.

Contents:

.

0. Motivation for a high field MO Kerr probe based on direct optics.

0.1 Global view.

Magneto-Optical experiments in high fields are done at almost all high field institutes. Mostly fiber-optics is applied to get the light to and from the samples. The large Faraday rotation in the fiber, in-coupling difficulties, possible fluorescence effects, the spectral attenuation of the fiber material, etc. etc. make accurate Kerr or Faraday experiments rather difficult and quantitative analysis almost impossible. Although MO measurements can be done by fiber optics, the author believes that a system using direct optics will have a lot of advantages and a superior performance.

The two laboratories with the most impressive high field MO Kerr equipment using direct optics are the Institute for Semiconductor-physics and Optics at the Technische Universität Braunschweig [12] (Germany, Prof. Schoenes) and the Institute for Solid State Physics at the University of Tokyo [13] (Japan, Prof. Miura).
The setup in Braunschweig was built by Keßler in the eighties [1,2]. They use a bitter magnet of 15 Tesla with a bore diameter of 53 mm. Measurements can be done in transmission or reflection mode. By different spectrometers the complete spectral range from 250 nm to 20 μm is covered. Focusing of the beam on the sample is done by mirror optics (openings angle = 1:10). The measurement principle is based on the vibrating halfshade polarizer technique (claimed accuracy 0.5 mdegree at 4 seconds integration time (see also section 2.1)). Low temperature experiments can be performed by using a cryostat with a bore of 20 mm [1]. The new setups in Braunschweig are equiped with an Helium gas flow cryostat. As the magnets are oriented with their bore horizontally, equipment can be built literally around the magnet. Although their magnetic fields are moderate, without any doubt the Institut of Halbleiterphysik and Optiks can be considered as the number one institute on MO Kerr spectroscopy in the world. Figure 0.1a shows a typical spectrum as measured with the equipment in Braunschweig [1].

At the University of Tokyo the Electromagnetic flux compression technique and the single turn coil technique is used in order to generate fields from 100 up to 550 Tesla for several microseconds (see also section 1.4). With the first technique the sample will be destroyed while the latter technique will spare the sample. Measurements are done with a laser via direct optics. Cryostats are made of plastic. The single coil technique experiments can be performed with a frequency of one shot / hour. The flux compression experiments take some more preparation (1 shot/day). The MO effect is measured in the

Faraday configuration by using a "crossed" polarizer and analyzer before and after the sample. The high fields make their equipment an excellent tool for the study of antiferromagnets (see Fig. 0.1.b).

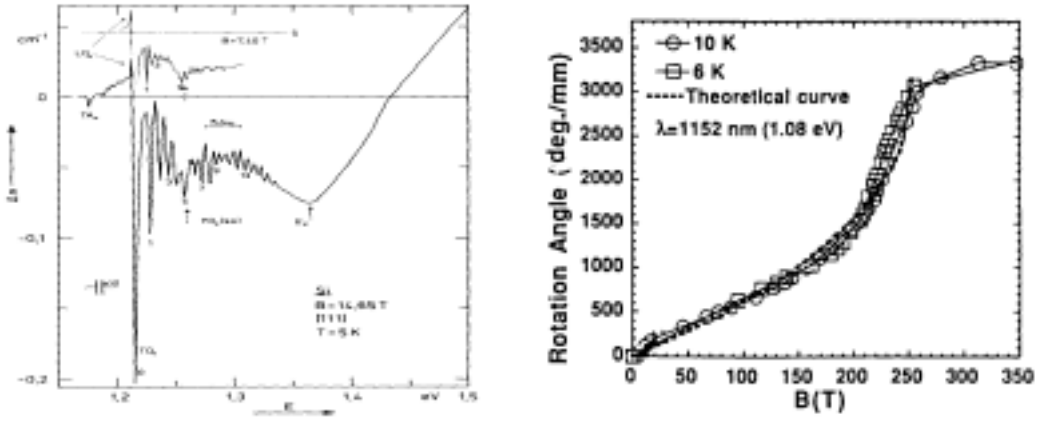

Figure Error! No text of specified style in document.**-1: (a) Fine structure of the MCD spectrum of silicon in the spectral region of the indirect adsorption edge: B=14.65 T and T=65K and T=5K [1]; (b) Faraday rotation angle in $CuFeO_3$ as a function of the magnetic field at a wavelength of 1.152 μm as compared with a theoretical curve [3].**

The overview given above suggests that a high field, low temperature, MO Kerr measurement system operating at DC-fields larger than 15 Tesla should be an excellent complement of worldwide existing equipment. Preferable Tallahassee should focus on the shorter wavelength range, as such equipment is lacking on the international scientific stage.

0.2 Local view.

At the moment three different types of magnetometers are in use at the NHMFL in Tallahassee:

a. VSM: accuracy 10^{-3} EMU: measuring of the flux changes sensed by a coil set by vibrating a sample with a magnetic moment.

b. AC susceptometer: accuracy 10^{-7} to 10^{-8} emu depending on the applied field.

c. Cantilever-Beam Magnetometer: measurement of the force or torque acted on a sample in an inhomogeneous or homogenous field. This value provides indirect a measure for the magnetic moment. A sensitivity of 10^{-7} to 10^{-9} is obtainable. The biggest problem with

this technique is that it requires samples smaller than 1 mm^3. So for most samples it is a destructive technique. Furthermore it might be difficult to do quantitative or qualitative analysis between different samples, especially in the case of thin films.
Above mentioned sensitivities are not fundamental ceilings. They apply for the equipment at the moment available at NHMFL. Most low field VSMs have an accuracy better than 10^{-5}, and "oscillating" cantilever Beam Magnetometers (Reed magnetometers) with an accuracy in the 10^{-11} to 10^{-12} have been built [4].

It is possible to apply the MO Kerr effect as a probe for the magnetization in the material. Prof.. Miura from Tokyo showed that on the one dimensional antiferromagnets a Kerr magnetometer can be a very strong research tool. Applying the Kerr effect to determine the hysteresis curve of ultra thin iron films (see also Fig. 1.8 of the user manual) would result in a technique with an accuracy better than 10^{-9} emu. We have to realize that this number does not have to be linear on the magnetization. In fact it is linear on the exchange coupling and spin orbit coupling of the iso-energy difference surface belonging to the wavelength of the light used in the experiment. Although a MO Kerr magnetometer is not supposed to solve all the problems, it will surely provide an easy, sensitive, and non-destructive technique to determine the hysteresis curve or probe indirectly the magnetization. Furthermore it will clearly complement the already available equipment in Tallahassee.

1. High field technology.

Although the generation of high magnetic fields should be evident in an institute as the NHMFL, the author believes that a short overview would serve the new users and those working in related fields. The specialists may omit this section.
At low power levels, of the order of kilowatts, the highest magnetic fields can be achieved with iron-core electromagnets, in which magnetizing fields are produced by coils surrounding iron poles. At higher power levels, it becomes important to use the power as effectively as possible. This is accomplished by using an air-core coil leaving room for access to the high field within the coil along the coil axis. Iron, if

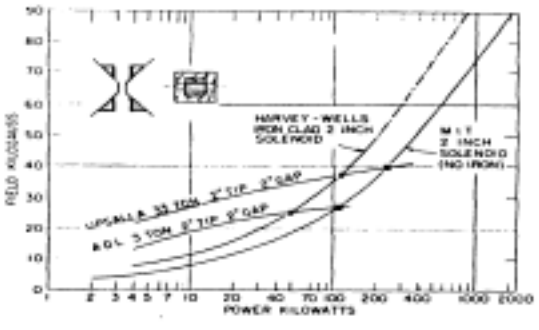

Figure 1.1: Field versus power in iron magnets, showing the crossover between convential iron core

used at all, becomes subsidiary in the form of a shell around the coil. The power above which an air-core magnet becomes preferable to an iron-core one is somewhere around 200 kilowatts (see also Fig. 1.1) [5,6,25].
Another important fact for the generation of high magnetic fields is the bore diameter. Basically, the smaller the bore diameter, the larger the field. So this forces the magnet-designer to find a compromise between available space and maximum obtainable field.

A lot of methods have been proposed to generate large magnetic fields. The most frequently will be shortly explained below.

1.1 Resistive Bitter magnets.

In resistive Bitter magnets, the windings are formed by perforated copper disks (see Fig. 1.2) [5,6,25] insulated from each other by mica plates. Successive copper disks slightly overlap and form a kind of spiral (a winding stairs around a central hole). The whole stack of copper and mica disks is pressed together to form a cylinder. All holes in successive disks are supposed to line up. The central hole is the bore while the smaller holes, off-center, are cooling channels. This cylinder is capsulated in a stainless steel skin. Lots of water is squeezed through the off-centered channels in order to cool the magnet. Two important design issues are the cooling power (how much heat can be removed by the cooling water) and the strength of the materials involved (large forces will work especially on the inner part of the bitter plates). The first issue is most important as it determines the maximum power which can be applied without melting down the “coil”. Increasing the number and diameter of the cooling channels will reduce the quantity of copper and thus increase the coil resistance. Somewhere there is an optimum for the number [5], diameter, distribution [6], and shape [7] of the cooling channels. Although the strength of the materials involved has never been a big issue, recently it becomes important in the magnet design. New alloys, like for example CuAg, might push the fields of next generation magnets a factor 2 or so. A bitter magnet provides a DC magnetic field superposed with a small AC field caused by the noise of the power supplies. The 40 MWatt

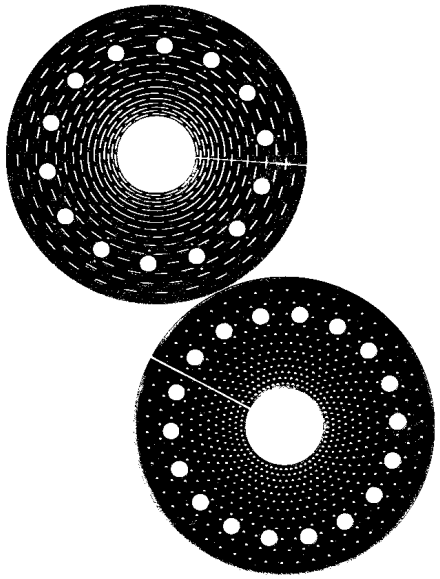

Figure 1.2: Two different types of Bitter disks

power supply at NHMFL has a noise level smaller than 1 ppm. The world record field which can be obtained by a resistive magnet is momentarily held by the NHMFL (33 Tesla).

1.2 Superconductive magnets.

With the current superconductive technology, magnets with maximum fields up to 22 Tesla have been built. Because the coils of these magnets do not have a resistance at low temperatures, the magnets can be charged with a small power supply. Keeping the magnet at maximum field does not cost you any energy except for the helium boil off. This makes this kind of magnets very attractive for experiments which require high fields over longer periods of time.
The main disadvantage of superconductive magnets is its slow ramping speed (0.5 Tesla / minute) compared to that of a resistive magnet (40 Tesla / minute). The ramping speed of a superconductive magnet is limited by the generation of eddy currents in its stainless steel jacket, and the possibility of quenching when the dB/dt and thus the induction current, or higher harmonics, will pass the critical current. When quenching the magnet all energy in the magnetic field will be dissipated in a very short time. This will result in a sudden increase of the temperature, will boil of the helium, and might generate a large induction voltage over the connectors of the magnet. All kind of pressure valves and protection diodes avoid real catastrophes when such an event occurs.

1.3 Pulsed Magnets.

By applying only a very short current pulse to a magnet, part of the heating problem is solved, and much higher currents can be applied. In this case the heat capacity of the coil and the rest of the construction is used. These magnets consist of wounded Cu (or CuAg) and fiber. The first for the current and the latter for the strength. The equipment is cooled by placing the whole coil in a liquid nitrogen bath. A short current pulse is caused in the coil by discharging a capacitor bank. Between two shots the magnet needs normally a cooling down time of one hour. Fields up to 60 Tesla for several milliseconds (non destructive) are possible at the NHMFL facilities in Los Alamos.
Another technique to create the high pulsed field is by supplying a short large current pulse with a half cycle of about 5 micro-seconds to a small single turn coil made from a copper plate. Very large fields up to 200 Tesla can be obtained for microseconds (bore diameter 6 mm) [3].

Probes designed for this or other AC-field experiments, can not contain any highly conductive materials like Al, Cu, bronze etc. etc.. The large dB/dt will generate eddy-currents in the metals which might lead to forces or heating. Also the use of highly conductive samples is a problem. The shape of the sample, i.e. a wire parallel or thin film parallel to the field, might solve some of the eddy current problems.

1.4 Flux compression.

Flux compression can be applied to generate magnetic fields up to 10 megagauss. A current is injected in a copper ring, what they call the liner. The ring is imploded while maintaining the current through it. Because the total area of the coil is decreased and the current does not change, the flux through the coil surface should stay the same. So the magnetic field within the coil will largely increase. The ring can be imploded by using for example explosives, or the electromagnetic forces between a primary coil and the ring. In the latter case we speak of electromagnetic flux compression. Fields up to 500 Tesla can be obtained with rise times of several micro-seconds. It is clear that these techniques are destructive. The big disadvantage is that it is no longer possible to repeat the experiment on the same sample under different experimental conditions (e.g. another temperature). The NHMFL in Los Alamos performs compression high field experiments using explosive. Fields up to 1000 Tesla can be obtained by this method [8].

2. Magneto-Optical Measurement technique.

In literature several different techniques have been suggested to measure the Magneto-Optical Kerr effects (reflection on ferromagnetic materials), the Faraday effects (transmission through ferromagnetic and non-ferromagnetic materials), and the Faraday reflection effect (reflection on non-ferromagnetic materials).

The most simple technique is to use an almost crossed polarizer and analyzer. When crossing both prisms at a large angle not too close to the extinction angle of 90 degrees, the intensity measured behind the analyzer will be linear with the polarization direction of the reflected beam [10]. Although the stability of the current generation of amplifiers and lasers is good enough to give a working setup (accuracy better than 1 mdegree), such setup should be avoided for high field applications. The high fields and field changes (dB/dt) associated with the large magnetic field generation technology, are expected to

influence the alignment of the setup and might reflect in large mechanical backgrounds with hysteresis (this suspicion was confirmed by the first experiments on MOK1 (see also chapter 4)). Another disadvantage of this DC technique is that wavelength dependent measurement are difficult. The light emerging from a monochromator is several orders of magnitude smaller than the usual milliwatts of a HeNe laser. After two practically crossed polarizers the remaining power is in the order of nanowatts, which imposes problems with the NEP of Si diodes with stray light [9].
For high field MO experiments it is preferable to use a kind of modulation technique. Several different devices have been proposed to modulate the State Of Polarization (SOP) of a monochromatic light beam. The most important ones, will be listed in the following two sections.

2.1 Mechanical Modulators of the State of Polarization.

The following mechanical modulators were found in literature.
a. Spinning analyzer prism: A Glan-Thompson prism is mounted in the shaft of an electric motor and rotated with a frequency of 30-60 Hz. Higher harmonic vibrations in the rotator limit the accuracy of the measurement system. Accuracies are typical in the order of 10 mdegree. Furthermore the use of an electric motor will make the measurement technique less suitable for high field applications and vacuum. The time response of the technique is between 15 and 30 mseconds. The advantage of the technique is that it will give the absolute value of the rotation. No calibration is necessary [10].
b. A vibrating half shade polarizer, consists of two Glan Thompson prisms oriented 90 degrees with respect to each other, mounted on two blade springs [2]. The blade springs are excited by two Piezo Keramik elements. Accuracies of 0.5 mdegree are feasible (integration time 4 seconds). The low modulation frequency (30 Hz) makes this technique less interesting for pulsed magnet experiments. The clear aperture is limited as the total mass can not be that large for a certain spring - frequency combination.
This type of modulator appears to work well in the stray field of a Bitter magnet.
c. Null method: An electric motor crosses an analyzer with the polarization direction of the reflected beam. In order to increase the sensitivity of the measurement technique, the polarization direction of the reflected beam is modulated by a Faraday cell. Accuracies below 1 mdegree are possible with such a technique. Because of the electric motor and the Faradaycell, the technique is unsuitable for high field applications, and because of the electric motor measurements in vacuum are difficult. The time response is typical slower than 0.3 seconds. A further disadvantage of this system is the maintenance the electric motor and transmission require. The first generation Kerr spectrometers of the Jasco

company were based on this principle. Prof. Lind's set up, although not completely automated, is also based on this principle [11].

Although sensitive low field setups have been built by using mechanical modulators, the author strongly believes that they should be avoided in a high field setup in Tallahassee. The low modulation frequency (just in the range where we expect a lot of noise originating from mechanical vibrations caused by the cooling water system of the magnets) and the fact that they are not commercially available make them less attractive over their electronic cousins.

2.2 Electronic Modulators of the State of Polarization.

With the electronic modulation techniques, accuracies in the sub-mdegree range can be obtained with reasonable integration times.
a. Faraday Modulators: (see also section 2.1) The cells are long, the wavelength range is limited, the modulator requires water cooling, and the modulator can not be used in the stray field of a large magnet.
b Pockels Cell: These modulators are based on the electro-optic Kerr effect. The cells are long (typical 3 cm). The long length make them less attractive to be used in combination with large magnetic fields. The advantage of this type of modulator is that basically all kinds of waveforms can be used up to several MHz which make them interesting for the pulsed magnets where a quick response is necessary.
c. Piezo-Optic or Photoelastic modulators: Piezobirefringence at the mechanical resonant frequency of a transparent bar is induced by mechanical stress: the modulator consists of a crystal which is sinussioidally expanded and contracted in one direction by a piezo electric actuator. Linear polarized waves with a polarization plane parallel to this direction are retarded when the element is expanded, and advanced when it is contracted. In this way a periodically varying phase shift is added. Linear polarized waves with a polarization plane orthogonal to the contraction direction are not influenced. The modulation frequency is typically around 50 kHz. The larger the frequency the smaller the clear aperture of the modulator.
The advantages of this type of modulator are a large clear aperture, a short light path, and a large radiation through put. In addition the modulator can be used over a wide wavelength range. Sensitivities of 0.05 mdegree [12] (integration time 3 seconds) are feasible. The disadvantage of a Kerr setup based on this principle is that the measured values are no longer absolute: calibration is necessary.

Considering the compilation above, we choose for the PEM modulation technique. The large clear aperture, the short light path, the applicability in high fields and vacuum, the large wavelength range, and its high frequency make it surely the most attractive choice for a magneto-optical measurement technique for a DC high field probe.

2.3 Measurement scheme based on the PEM.

The MO setup is given in Fig. 2.1. Light from a HeNe laser is deflected by a mirror A. We choose for a horizontal laser plateau in order to simplify magnetic shielding (see section on shielding) and open the opportunity to exchange the HeNe laser (2 eV) with a HeCd laser (lines near 3 and 4 eV: It is not possible to position a HeCd laser vertical as the mirrors will be contaminated with Cd) The drawback of this setup is its asymmetry: via the stray field this could lead to horizontal forces, which because of the long length of the probe could add up to large torques. The HeNe laser is a stable linear polarized light source. The latter is necessary for the use in a polarized setup. Using a non-polarized laser would result in large intensity changes after the polarizer [13].
After reflection with the mirror (A), the laser beam is polarized by a Glan-Thompson prism (B) and modulated by the Photo-Elastic Modulator (C). The light incident on the PEM is polarized at 45 degrees with respect to its optical axis. If the modulation depth of the PEM is a quarter labda, the transmitted light will become alternately right-handedly and left-handedly polarized (50 kHz).
From the modulator the light will have to travel two meters down to the sample. Because of the length of the light path and the large fields involved, it is expected that the Faraday effect of the air will give rise to a rotation of around 0.44 degrees (based on a wet finger calculation and the Verdet constants of air as given in the Handbook of Physics and Chemistry). In order to avoid this background most of the light path must go through vacuum. The vacuum window (D) of fused silica (negligible birefringence) is positioned at 2 meters from maximum field, approximately 1 meter above the cryostat. At one meter from maximum

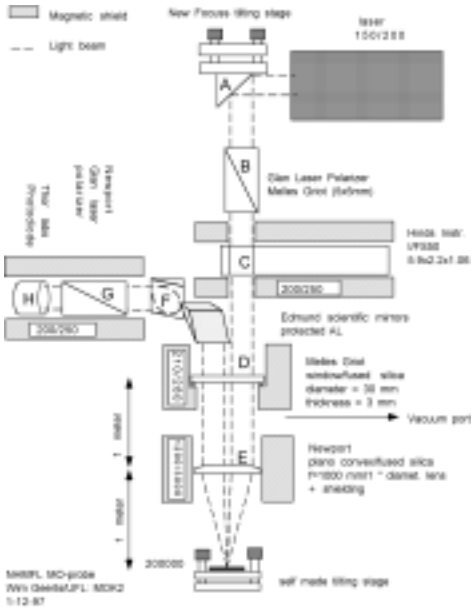

Figure 2.1: Scheme of the optics of MOK3 (for an explanation of the labels see

field a plano-convex lens (E) is situated. The lens is made of fused silica and has a focal length of 1 meter. This should provide sufficient focusing power in order to keep the laser beam diameter smaller than 2 mm. If smaller spot diameters are necessary it is possible to include a pin-hole with two lenses on top of the laser platform. In exchange for light intensity a smaller spot-diameter can be realized. Both the lens and the vacuum window are from fused silica. This material has a very small optical birefringence.
The angle of incidence with the sample is smaller than 0.33 degrees. In this configuration the Polar Kerr effect is measured (field perpendicular to the sample surface). From the three Kerr effects, i.e. longitudinal, transverse and polar, the last one is the largest. Because of the non-zero off-diagonal components of the dielectric tensor [14], the state of polarization of the reflected beam will be slightly affected. The reflected beam is no longer perfectly modulated between right and left handedly circular polarized light. The way the state of polarization (SOP) of the light beam is changed after reflection with a

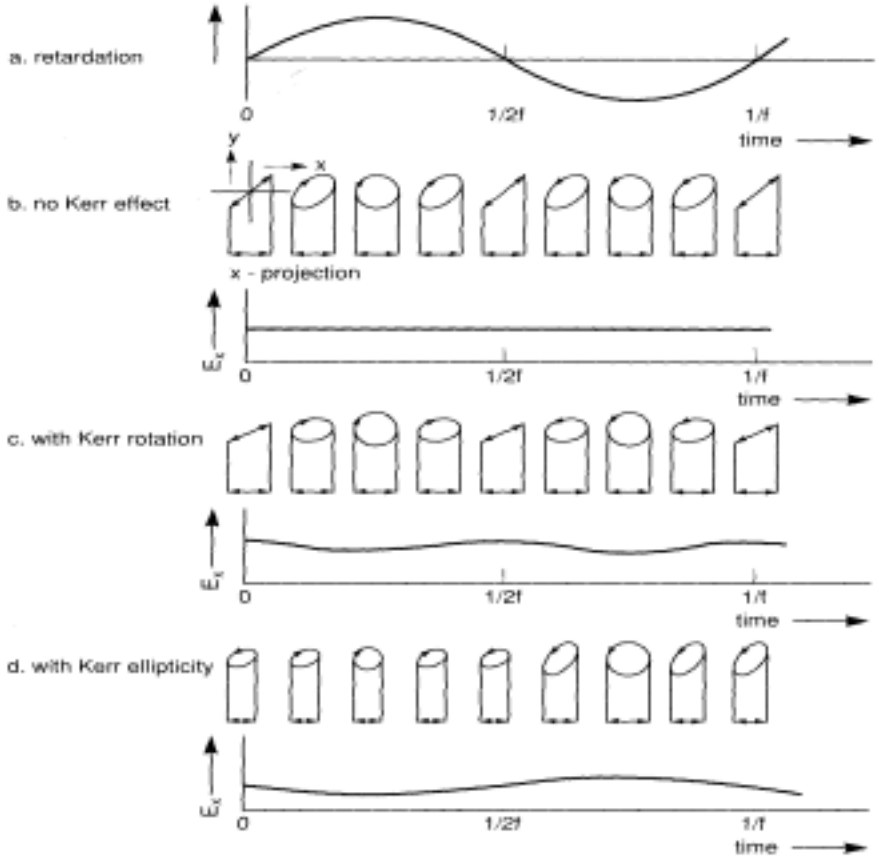

Figure 2.2: retardation δ as a function of time, (b) polarization state of corresponding light vector, (c) as (b) but after introduction of Kerr rotation, (d) as (b) but after introduction of Kerr ellipticity

ferromagnetic material is shown in Fig. 2.2 [14]. This change is detected by another polarizer prism (Glan Laser polarizer (G)), and a detector with transimpedance amplifier (H). The light beam is deflected by a set of two mirrors (F), which optical axis are rotated over 90 degrees with respect to each other. The s component of the first mirror coincide with the p-component of the second mirror. This mirror pair has a transformation matrix which is 1 for whatever wavelength. It will avoid the introduction of non-linear effects as described in [15]. This is a big advantage in the case one is interested in the absolute values of the Kerr effects.

The clear aperture was made as large as possible: this in order to ease the alignment procedure and to reduce mechanical induced intensity variations. The mechanical vibration of the cooling water circuit of the magnet and the slight bending of the probe under the magneto-static forces will lead to small beam displacements during the measurement. As long as the displacements are smaller than the clear aperture, they will not induce intensity variations. Part of this is due to the small angle of incidence. At 0.3 degrees, the Fresnell coefficients hardly depend on the angle of incidence. For most low field setups (angle of incidence is 10-15 degrees, this is not the case. The clear aperture of MOK3 was 1 cm^2 with exception of the polarizer. A 0.5x0.5 cm^2 polarizer was used because of its short length (lens shielding problems). As the laser polarizer distance is less than 10 cm this will not limit the performance. For the analyzer a 1 cm^2 Glan Laser prism was used. The magnetic shielding of the analyzer is easier because the magnetic field is perpendicular to its optical axis. The silicon detector has a surface are of 13.7 mm2 which was the maximum availlable at Thorlabs Inc. In order to avoid above described "parasitic" diaphragm effects, the reflected laser beam was focused on the silicon detector by a lens with a focal length of 0.5". As this lens is placed behind the analyzer it can be a cheap glass lens. The

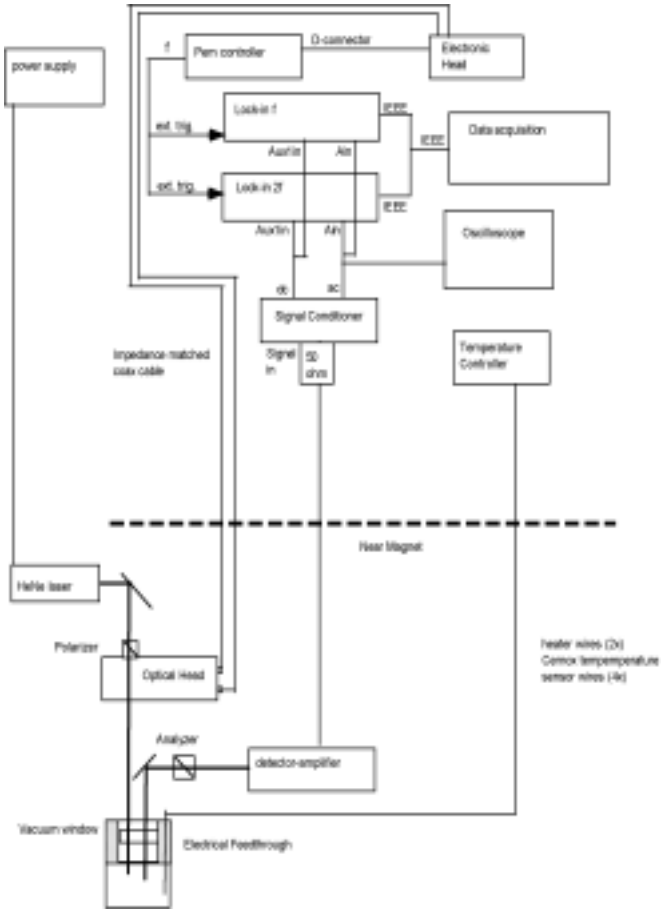

Figure 2.3: Electronic setup of MOK3

spectral responsivity and the bandwidth of the detector are given in appendix 1. It should be mentioned here that the gain should be kept low in order to guarantee an equal amplification factor for the ω and the 2ω signal (ω = 50 kHz) (see also section 2.4).

As shown in Fig. 2.2, the Kerr rotation and Kerr ellipticity can be determined by measuring the 2ω and ω component on the detector signal (ω is the modulation frequency of the PEM). This can be done by using two lock-in amplifiers. The following section will give a mathematical description of the measurement technique based on Jones calculus. The setup of the electronics is given in Fig. 2.3.

2.4 Mathematical description of the measurement technique [16].

The amplitude of the detector signal can be determined by means of a Jones matrix calculation [26]. It has been shown that polarized light can be written as the sum of two linear (or circular) polarized beams. The state of polarization of the light depends on the phase difference and the amplitude ratio of both linear polarized components. In this section the detector light is resolved in a component parallel and perpendicular to the modulation axis of the PEM (see also reference [26]). Both components are complex and the total can be written as a vector. The polarization of the light in front of the detector can be calculated from the transfer functions of all the optical components. E_{det} can be written as:

$$\vec{E}_{det} = \begin{pmatrix} \tilde{E}_{dx} \\ \tilde{E}_{dy} \end{pmatrix} = A \cdot R \cdot T_{c-c} \cdot M \cdot \vec{E}_{in} \qquad \vec{E}_{in} = \frac{1}{\sqrt{2}} \begin{pmatrix} 1 \\ 1 \end{pmatrix}$$

where E_{in} is the description of the light in front of the photoelastic modulator (in cartesion coordinates). The x and y component have equal amplitude and are in phase. The other matrices describe the optical transfer functions of the components in the light path. They will be described below. The Jones matrix for the modulator M is:

$$M = \begin{pmatrix} e^{i\delta/2} & 0 \\ 0 & e^{-i\delta/2} \end{pmatrix}$$

with δ being the retardation, which is periodic in time t:

$$\delta = \delta_0 \sin(2\pi p t)$$

with δ_0 the amplitude of the retardation and p the operation frequency of the PEM. It is convenient to transform from cartesian to circular coordinates by the transformation matrix $T_{c\text{-}c}$:

$$T_{c-c} = \frac{1}{\sqrt{2}} \begin{matrix} 1 & i \\ 1 & -i \end{matrix}$$

The Jones matrix for the reflection at the sample is:

$$R = \begin{matrix} \tilde{r}_+ & 0 \\ 0 & \tilde{r}_- \end{matrix}$$

$$\tilde{r}_\pm = r_\pm e^{i\phi_\pm}$$

where the latter represents the complex Fresnel reflection coefficients of the samples.
Finally, the Jones matrix for the linear analyzer is, in circular coordinates:

$$A = \frac{1}{2} \begin{matrix} 1 & e^{-2i\phi} \\ e^{2i\phi} & 1 \end{matrix}$$

with ϕ the azimuth of the transmission axis with respect to the x-axis (=modulator axis). It is not necessary to transform back to cartesian coordinates since the intensity of the light beam I is insensitive to that:

$$I = \left|\dot{E}_{\det}\right|^2 = \dot{E}_{\det}^{\ *} \cdot \dot{E}_{\det} = \tilde{E}_{dx}^{\ *} \cdot \tilde{E}_{dx} + \tilde{E}_{dy}^{\ *} \cdot \tilde{E}_{dy}$$

where the asterix denotes the complex conjugate. Straightforward calculations yields:

$$I = \frac{1}{4}\left[r_+^{\ 2} + r_-^{\ 2} + \left(r_+^{\ 2} - r_-^{\ 2}\right)\sin\delta + 2r_+ r_- \cos\delta \cdot \sin\left(2\phi + \phi_+ - \phi_-\right)\right]$$

with $\phi_+ - \phi_- = 2\theta_k$ (which is valid as long as $(r_+ - r_-) << (r_+ + r_-)$). This expression for I can be approximated by:

$$I = \frac{1}{2}R\left[1 + 2\eta_k \sin\delta + \cos\delta \cdot \sin(2\phi + 2\theta_k)\right]$$

with $R=1/2(r_+^{\ 2} + r_-^{\ 2})$, η_k the Kerr ellipticity, and θ_k the Kerr rotation. Both $\sin\delta$ and $\cos\delta$ can be expanded into Bessel functions (see Fig. 2.4). Straightforward calculations (neglecting the higher harmonics) shows that the intensity consists of the frequency components:

$$I = I(0) + I(p)\sin(2\pi pt) + I(2p)\sin(4\pi pt) +$$

where:

$$I(0) = \tfrac{1}{2}R\left[1 + J_0(\delta_0)\sin(2\theta_k + 2\phi)\right]$$

$$I(p) = \tfrac{1}{2}R\left[4\eta_k J_1(\delta_0)\right]$$

$$I(2p) = \tfrac{1}{2}R\left[2J_2(\delta_0)\sin(2\theta_k + 2\phi)\right]$$

which except for the missing I_0 and the factor 1/2 is the same as the expression in the user manual. The I_0 is related to the laser intensity while in the calculations presented here we assumed a laser intensity of one. (see the definition of E_{det}).

Assuming that the amplification factor for the ω and the 2ω component are the same we may write:

$$\frac{I(p)}{I(0)} = BJ_1(\delta_0)\frac{\Delta R}{R} = 4BJ_1(\delta_0)\eta_k = A_{ell}\eta_k$$

$$\frac{I(2p)}{I(0)} = BJ_2(\delta_0)2\Delta\theta = -BJ_2(\delta_0)\theta_k = A_{rot}\theta_k$$

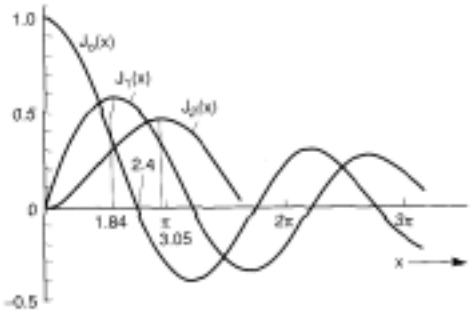

Figure 2.4: Bessel functions J_0, J_1, and J_2

with B the ratio between the AC and the DC amplification of the silicon detector amplifier and the signal conditioner, η_k the Kerr ellipticity, θ_k the Kerr rotation, and A the calibration factor. So by dividing the ω and 2ω component by the dc component we can get rid of the laser noise and other intensity variations. This is important as the water-cooling system of the magnet causes the whole probe to vibrate with a frequency of 20-200 Hz. These vibrations together with a slight bending (see chapter 4) of the probe at higher fields, might introduce intensity variations of a magnitude comparable to the MO component of the detector signal.

The value of the B factor can be set by the HINDS signal conditioner used in the electronic set-up. This is an broadband amplifier with an AC and DC leg. The amplification of both legs can be set independently. The whole MO system can be calibrated by the ratio of both amplification factors.

From the equation above we can also see that the sensitivity depends on the modulation depth δ_0. By changing it we can maximize the S/N

ratio of the quantity we are most interested in or we can choose that value for which the calibration factors are equal for both quantities. The table below gives the calibration factors for some different modulation depths.
We note that ηk can be obtained without inserting an analyzer. Omitting A from the first equation of this section yields for I:

$$I = \frac{1}{2}\left[r_+^{\,2} + r_-^{\,2} + \left(r_+^{\,2} - r_-^{\,2}\right)\sin\delta\right]$$

Table 1: Calibration ratios for different modulation depths.

δ_0	description	A_{rot}	A_{rot}/A_{ell}
$\pi/2$	maximum 1ω sensitivity	0.3	0.5
2.4	real DC signal	0.4	0.3
2.6	$J_1(\delta_0) = J_2(\delta_0)$	0.45	0.25
π	maximum 2ω sensitivity	0.5	0.2

So also in this case the w signal represents the Kerr ellipticity. The detector signal, however, is twice as large as withoug the analyzer inserted. This can be exploited if the Kerr signals are small and if one uses the Kerr effect only as a tool to probe other magnetic properties, such as hysteresis loops, Curie temperature or magnetic anisotropy. Then measuring η_k without an analyzer instead of θ_k yields a better signal-to-noise ratio in the experiment, provided that η_k is not much smaller than θ_k.

3. Magnetic Shielding.

3.1 Shielding methods.

Three type of magnetic shielding technologies have been proposed in literature:
1 Passive shielding by ferromagnetic materials.
2. Shielding by superconductors.
3. Active shielding by coils.
The disadvantages of the second technique are that you need low temperature, that the materials involved are brittle and not easy to machine, and that only small ramping speeds

may be applied (see also section on superconductive magnets). The disadvantages of the third method are the limited field that can be generated with an air cooled air-core coil and the necessity for an extra power supply with all kind of protection units to avoid calamities when the bitter magnet trips. Higher fields can be generated by using extra iron as a coat around the coil, however this does not simplify the technique.
For these reasons we choose for the passive shielding option with ferromagnetic material. As the coercivity of most materials increases with decreasing temperature, we have to be sure that the shields stay at room temperature to assure optimum performance. For this reason we have to be sure that the shields stay around room temperature when measuring at low temperatures.

3.2 Passive Shielding.

Magnetic shielding of low static and alternating fields is well understood and widely applied in order to shield cathode ray tubes and photo-multipliers from disturbing magnetic fields. Several companies offer their services and design custom solutions based on the theory developed by Albrecht Mager [17, 18, 19] and others in the seventies and the usage of thin sheets of μ-metal. This material has a very high permeability (only at low fields), and a low coercivity. Its low saturation magnetization, high price, and the expensive treatment are however clear disadvantages. Shielding of higher fields is possible, but commercially less attractive. In that case you need to use material with a larger saturation magnetization and/or need to use more material. The latter and also the presence of the larger fields, and thus larger derivatives of the field, make it necessary to use stronger constructions. The basic principle of high field shielding is not different from its low field brother:
1. Inductive explanation: the object to be shielded needs to be surrounded by a magnetic material which is a good conductor of the magnetic induction and depletes the field around it. The shielding material can be considered as a kind of vacuum cleaner for magnetic field lines. Maximum absolute shielding will be otained when the shield saturates.
2. Magnetostatic explanation: the object to be shielded needs to be surrounded by magnetic material which acts as a magnet and compensates the magnetic field at the position of the object. This compensating field is similar to the demagnetizing field working on a magnetic bubble in a thin film. Maximum absolute shielding will be obtained when the shield resembles the geometry of a thin film with a small hole in it. The maximum shielding will be reached when the shield saturates.

REMARKS:

1. “Absolute shielding” is the decrease of the external field at the location to be shielded (different from the shielding efficiency” parameters, used by the shielding industry, which is a relative parameter).
2. The shielding field depends on the material but can be largely influenced by the design. This becomes clear when we compare a hysteresis curve of bulk material with that of a thin film (the famous shearing of the hysteresis curve depending on the demagnetizing factor of your object). Demagnetizing forces counter act the external field and keep the permeability low at low fields but non-zero at high fields. By shaping the shield it is possible to obtain saturation fields close to the saturation magnetization of the material (thin film limit).

The total amount of shielding material should be as small as possible, and certainly not extend several kg: we do not want the probe to become too heavy, and more important, we do not want to introduce too large magneto-static forces on the probe (it may be evident that shields, magnetic objects, will lead to forces in the non-homogeneous stray field of the Bitter magnet. In order to get some idea about the shielding efficiency of a cylinder oriented parallel to the field the following calculations were performed:
Assume a cylinder of magnetic iron with inner diameter R1, outer diameter R2, and length L is placed in a magnetic field, H. The field will magnetize the cylinder. The magnetic charges at the top and bottom of the cylinder will cause a demagnetizing field in the cylinder wall. This demagnetizing field will prevent that the shield material will saturate at low external magnetic fields. As long as no saturation will occur, the total internal field in the cylinder wall (=external field + demagnetizing field) will be close to zero (in fact close to the saturation field of an infinite rod of the same material). Calculations show that the field at the axis of the cylinder and the field in the cylinder wall are of the same order of magnitude: this explains the shielding effect.
Rough estimations have been performed in order to estimate the maximum absolute shielding. For this we assumed that the cylinder was homogeneous magnetized along its axis. Its compensating field along the axis of the cylinder is given by the following equation:

$$H_d(z) = \frac{1}{2} M_s \left[\frac{z}{\sqrt{\frac{L^2}{4} + R_1^2}} + \frac{L - z}{\sqrt{(L-z)^2 + R_1^2}} - \frac{z}{\sqrt{\frac{L^2}{4} + R_2^2}} + \frac{L - z}{\sqrt{(L-z)^2 + R_2^2}} \right]$$

where Ms is the saturation magnetization of the shield, L its length, R1 its inner diameter, R2 its outer diameter, and z is the position along the cylinder axis. In the middle of the cylinder the compensating field will be:

$$H_d(L/2) = \frac{1}{2}M_s \left(\frac{L}{\sqrt{\frac{L^2}{4} + R_1^2}} - \frac{L}{\sqrt{\frac{L^2}{4} + R_1^2 + 2R_1\Delta R + (\Delta R)^2}} \right)$$

The results are shown in Fig. 3.1. The y-axis gives the maximum compensation field divided by the saturation magnetization of the shield. An optimum exists for the ratio L/R1. Choosing R1=1", R2=2", and L=2" will give a shield with a maximum shielding capacity of 0.25Ms. Using carbon steel the maximum shielding will be somewhere around 5 Kgauss. In reality however, the cylinder will not be homogeneously magnetized. So this means that the magnetic charge will be distributed over the complete cylinder length. This will lead to an effective decrease of its length by approximately 33 %.
By a more extensive numerical calculations, it can be shown that the field in the wall of the cylinder is almost equal to the field on the axis (at least for z=L/2). The magnetic field in the material should be close to zero, as long as the shield does not saturate. This explains roughly the working of the cylinder shield.
It should be mentioned here that a cylindrical shield is not perfect, i.e. the sum of external field and compensation field is not zero, and more important it varies along the tube radius. A perfect shield should have the shape of an ellipsoid. This is however almost impossible to manufacture.

Shielding with the external field perpendicular to the cylinder axis is easier and more ideal. In this case the shielding is better understood by an inductive explanation. As a rule of thumb one often assumes that the field is strongly reduced in an area of two times the shield diameter as long as the material does not saturate. More information can be found in the papers of Mager et al. [17,18].

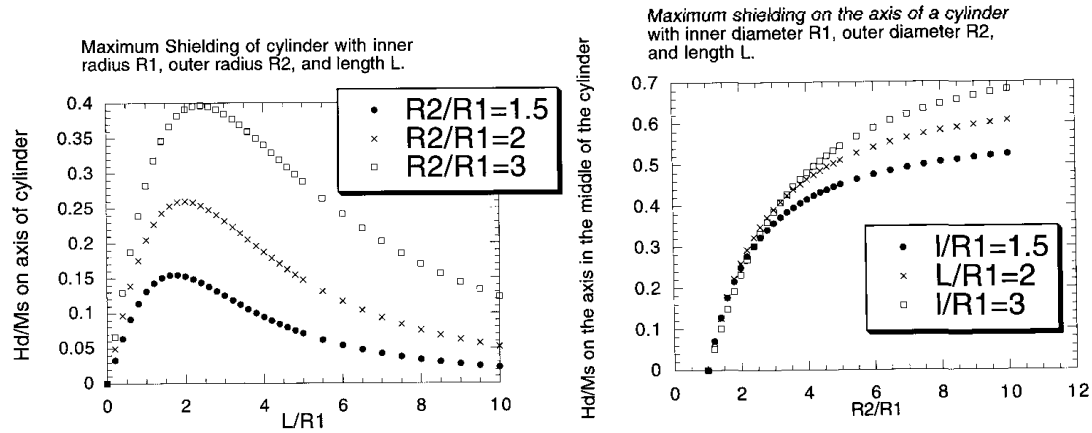

Figure 3.1: Performance of a cylinder shaped magnetic shield (field parallel to the axis): R1 is ID, R2 is OD, L=Length, Hd maximum compensating field on the axis in

3.3 Realization.

The following materials were used for magnetic shielding:

- μ-metal (a sample of amuneal Inc).
- magnetic iron: this material is very similar to carbon steel, C1018, however has a much lower carbon concentration and thus a lower coercivity. The specifications of magnetic iron are given in appendix 2.

Figure 3.2 gives an overview of the fields to be expected, the MO background to be expected without magnetic shielding, and the designed shields for the MOK3. The expected rotation background was calculated from the field distribution along the axis of the magnet and the Verdet constants as found in [27].
The efficiency of the PEM shield and analyzer shields were measured with a Lakeshore gaussmeter. The analyzer shield could not be saturated in the stray field of the magnet. The field inside the shield was smaller than 4 Gauss at an external field of 400 Gauss. The PEM shield saturates between 20 and 37 gauss. At an external field of 37 gauss the magnetic field in the shield is smaller than 12 gauss. At an external field of 20 Gauss, the magnetic field in the shield was smaller than 3 gauss. It should be worthwhile to make a thicker shield of magnetic iron for the PEM/polarizer unit.

The efficiency of the vacuum window shield and the lens shield have not been determined yet.

Preliminary measurements show that the background in vacuum is at least much smaller than 2 mdegree/Tesla. The rotation background in air is 20 mdegree/Tesla. The backgrounds on the ellipticity signal are much smaller and have not been determined yet. Preliminary results show a kind of asymmetric behavior Measurement of the high field susceptibility as a function of the probe position above and below the maximum might make it possible to separate contributions from the sample and the optics. Experimental preparation are in progress.

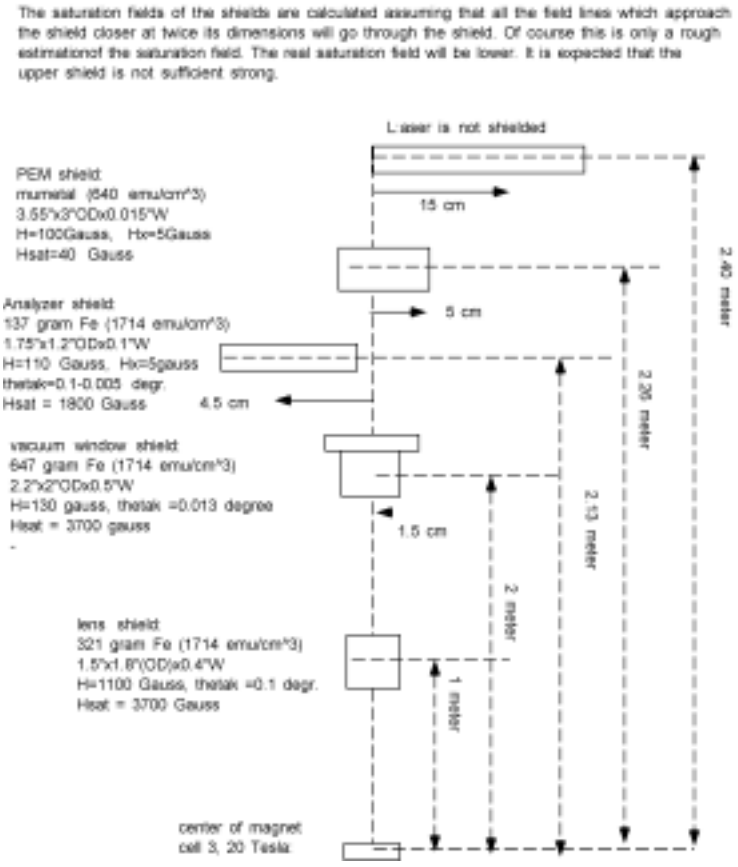

Figure 3.2: Magnetic shields for MOK3 and their predicted

4. Forces and Mechanical Stability.

The mechanical rigidity, not the shielding of the optical components, appeared to be the most important design factor. In order to understand this we have to realize that the total length of the light path is approximately 5 meters. A change of the sample orientation of only 0.03 degrees will result in a shift of the reflected beam of 1 mm. Such a shift can result in large changes of the measured intensity. Although the measurement technique as a first approximation should be independent of the intensity (see also section 2.4), large intensity variations will cause noticeable error signals. This will result in a so called mechanical background which in most cases is not linear with the field and shows hysteresis and a kind of random behavior.

Our first prototype, MOK1, appeared to be too sensitive to the magnetic stray fields of the magnet, and miss sufficient rigidity to resist bending. Ramping of the field from 0 to 20 Tesla resulted in a shift of the reflected laser beam of 3 mm: the mechanical background

was more than 3 times larger than the sample signal. Figure 4.1 shows the magnetic stray field on the axis above the magnet. Figure 4.2 shows the B and BdB/dz in the bore of the magnet. At those z-positions where the latter function is large, large forces are expected to work on the probe.

Two properties of the probe are important to avoid above described effects:

a. The sensistivity to the stray fields of the magnet.

b. The rigidity of the probe.

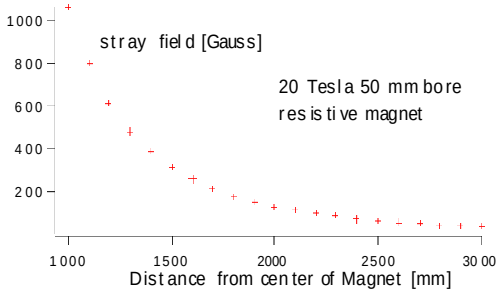

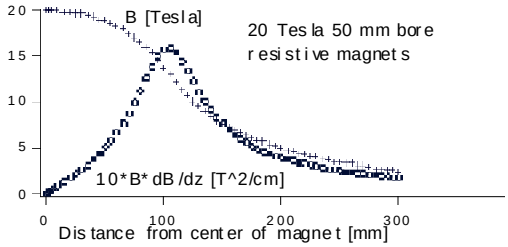

Fig. 3.1: Stray field along the axis above the 20 Tesla magnet; Fig. 3.2: B and B.dB/dz along the axis of the 20 Tesla magnet.

4.1 he sensitivity to the stray fields of the magnet.

The sensitivity of the probe to the stray fields of the bitter magnet depends on the used materials and the way they are manufactured. Coupling with the mechanical domain takes place in two ways:
1. Via the residual magnetic moment of the material: Copper, brass, and aluminum are slightly paramagnetic. Their magnetic moment depends on their impurity concentration. The magnetic moment of pure (oxygen free) copper is believed to be the lowest of the three.
304-Stainless steel is slightly paramagnetic at room temperature. At low temperature its magnetic moment largely increases. Bozorth mentions that the attractive force can be detected by hand in the strong field-gradients of a large electromagnet [20]. The scarce data available of the permeability at low temperature, suggests that 316-stainless steel would be a better choice for the low temperature range.
When stainless steel is hardened by cold work, some of the ferromagnetic alpha-phase precipitates. For this reason stainless steel tubes, stainless steel screws and machined stainless steel parts are ferromagnetic. Figure 4.3 shows the magnetic moment of a 304 stainless screw as measured by SQUID. Both a ferromagnetic and paramagnetic part are observed. The latter one increases largely (x7 for 20 tesla) when lowering the temperature till 10 K.

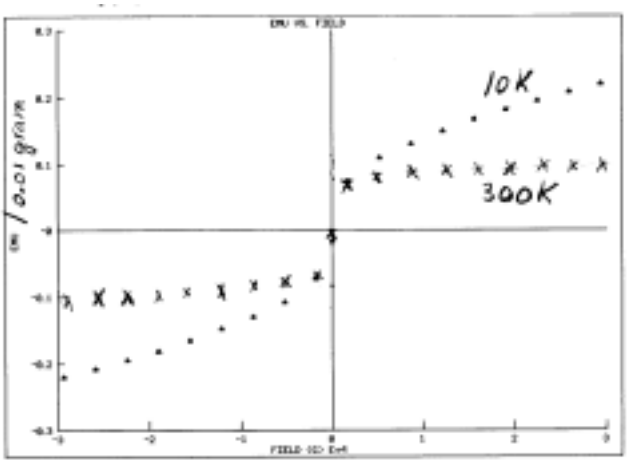

Figure 4.3: Magnetic moment of a stainless steel 304 screw measured at 300 K and 10 K.

The ferromagnetic moment in machined stainless steel can be removed by heating up till 1200 Celsius, and quenching it to room temperature. Preliminary experiments in Gainesville (quenching in water) showed that the flip over field of 304 stainless steel screws (field for which the screw is attracted to one of the pole pieces of an iron-core magnet) can be increased by a factor 2-3 by this treatment. Better results are expected when quenching in oil.
It is possible to order 316 stainless steel screws which are non-magnetic [21], however not all sizes can be delivered for a reasonable price.

All the machined stainless steel parts of the probe appeared to be magnetic at room temperature (attracted by NbFeB magnet). The first prototype, MOK1, contained a lot of machined stainless steel parts. All these parts in the bore of the magnet were removed in the second prototype, MOK2, in order to reduce the sensitivity to the stray fields.

The other way in which coupling takes place with the mechanical domain is via the induction of eddy currents in the materials involved. Eddy currents are due to field changes caused by ramping and/or the noise of the power supplies. Furthermore the mechanical vibration caused by the cooling circuit of the magnets will also cause dB/dt values unequal zero and lead to the generation of eddy currents.
The effect can be felt when moving a good conductor between the pole pieces of an iron-core magnet. As long as the object moves, an opposing force will act on the sample. The effects will be large for very good conductors like copper and aluminum, and smaller but still noticeable for brass. It is not clear to me whether or not these effects will cause large forces on the probe. Eddy currents will be surely important for probes for the pulsed magnet facility in Los Alamos. The dB/dt for pulsed magnets can be quite large. For probes for this facility, there is a design rule that one can not use copper, aluminum or bronze in the core of the magnets. Cryostats are normally made of plastic. For samples with large conductivity special precautions should be taken. A thin film or wire can be aligned parallel to the field, some films can be laminated, or nanostructured.

4.2 The rigidity of the probe.

Most of the probes used at NHMFL can be considered as a cantilever beam which is constricted on one side. The rigidity of such systems can be easily calculated from materials properties and dimensions of the system [22].
The deflection of such a system is expressed by:

$$D_B = \frac{P * l^3}{3 * E * I}$$

where D_B is the deflection at the free end-point of the beam, l is the length of the beam, E is the elasticity modulus, and I is the momentum of inertia.
The momentum of inertia for a tube with a wall thickness t, and a diameter d is given by the following expression:

$$I \cup \frac{d^3 * t * \pi}{8}, t << d$$

With the help of above two equations, the rigidity of the probe can be optimized. Considering the elasticity modulus, stainless steel (200 GPa) is a good choice. The elasticity modulus of aluminum (75GPa), copper or bronze (100 GPa) are much smaller. Better would be SiC (400 GPa). However price and expertise make this a less attractive move.
Except for increasing the wall thickness, increasing the diameter and reducing the length, the rigidity can be increased by constricting the beam on both sides, or at least at more points. This will give an effect comparable with decreasing the length.
From a more general equation of the momentum of inertia [22], it can be concluded that the tube is the geometry with the largest isotropic rigidity if the total amount of mass and space is limited. So it does not make any sense to look for bars or stars or whatever other shape. More information can be found in [22].

In the first prototype, MOK1, the rigidity of the probe appeared to be the major problem. Although the probe was supported at the top and the bottom by the vacuum can, the lens unit could move freely. MOK1 had a mechanical background of over 300 mdegree. In order to make the probe stronger, in MOK2 we incorporated an extra constrictor. This was a tapered ring which constricted the movement of the probe at the top of the tail of the vacuum jacket. So the probe was mechanically supported by the vacuum jacket at three different points: at the top via the Quik connector, at the top of the tail via the constrictor, and at the bottom of the vacuum jacket via the screw connection.
The first constrictor, an aluminum tapered ring, appeared to work well. The mechanical background of MOK2 was negligible. There are however two problems with this type of constrictor. Every time the probe is used the wedge on the aluminum ring deforms a little bit. This deformation is caused by the small space available between the probe and the vacuum jacket (0.035” of which 0.017” is available for the ring type constrictor). MOK2 does not work at low temperatures. Because of differential contraction between probe and vacuum jacket the mechanical support is lost when cooling down to liquid helium temperatures. The vacuum jacket contracts 2 mm more than the probe. The probe will be pushed up during the cool-down cycle and the constrictor will be no longer in its place. It is possible to tighten the probe at liquid helium temperature. However as soon as all the liquid helium is used, the vacuum jacket will expand faster than the probe and tear the lower part of the lower course of the probe apart.
These problems are solved in MOK3 by replacing the screw connection at the bottom by a spring locked tapered pin. This construction does not allow any movement in the x-y-plane while the probe can move freely along the z-axis (along the bore direction). The movement in the x-y plane is stopped by a 100 Newton brass spring. In MOK3 the

aluminum ring constrictor was replaced by a stainless steel clip constrictor. Because of the clip-construction we could use the full 0.035” available. Although stainless steel is slightly magnetic, the position of the constrictor, just below the lens unit, is far from the large B*dB/dz area. The constrictor clip has a very slow slope (3 degrees) which makes it self-locking. This new constrictor appears to be strong enough and will no longer deform during usage.
After putting the probe in the vacuum jacket the latter should be evacuated. The 30 pounds force resulting from the difference in pressure on both sides of the vacuum window will lock the constrictor and assure a tight construction. Because of those three points of mechanical support (Quik-connect at the top, constrictor at the beginning of the tail, and center unit at the bottom) the assembled probe will have a rigidity close to the rigidity of the vacuum can.

5. Thermal properties.

The MO Kerr probe was designed to work at least over a temperature range of 2-325 K. In order to guarantee reasonable thermal time constants and Helium boil of rates, rough estimations of the thermal properties were made in advance. In this chapter the thermal conductivity, heat capacity, thermal contraction and expansion, and eddy current heating will be discussed.

5.1 Thermal conductivity.

The thermal conductivity, k_t, of the probe determines the helium boil of, the thermal time constants, and the lowest obtainable temperature. It is defined by the following equation:

$$k_t = -\frac{\frac{dQ}{dt}}{A\frac{dT}{dz}}.$$

where A is the cross sectional area, dQ/dt the heat transferred per unit time, and dT/dz is the thermal gradient.
The thermal conductivity depends on the material and the temperature. Table 2 gives the thermal conductivities of copper, brass, stainless steel, and nylon. The latter should be close to the thermal conductivity of G10, for which no literature values could be found.

Table 2: Thermal conductivity (all values in W/cm.K) [23].

Material	k_t | 300K	k_t | 4K
oxygen free copper	5	80
aluminum	2.5	0.6
brass	1	0.03
stainless steel 304 (18-8)	0.15	0.0025
Nylon (close to G10)	0.0025	0.00015

The sample stage unit was made completely of copper in order to avoid temperature gradients. Both copper rings (see technical drawings) can be replaced by G10 versions. The G10 version will act like a thermal resistor and make temperature control possible over a wide range. Figure 5.1 is a thermal model of the probe. The numbers refer to the estimated reciprocal thermal conductivity all in K/Watt. The first number is the 4K value and the second the value at 300K. For Fig. 5.1 it is assumed that the probe is in high vacuum. Furthermore we neglected the conductivity of the copper heater wires, and the phosphor-bronze sensor wires.

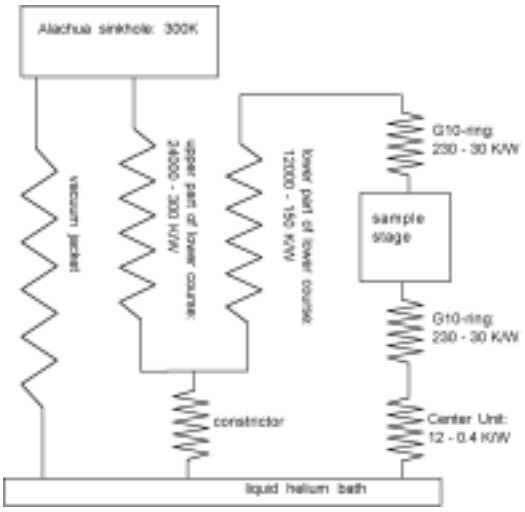

Figure 5.1: Thermal model of the probe.

The sample stage is heated by three heat sources:

- the HeNe laser and possible stray light which can hit the sample via the vacuum window.
- the 5 Watt heater just under the sample table.
- eddy current heating in the copper sample stage.

A rough calculations shows that the heat exchange between the vacuum window and the substrate is in the sub μWatt range. The long length of 2 meters acts as a kind of diaphragm. The light of the laser has an intensity in the mWatt range. This will cause a temperature drop of 2-4 Kelvin over the G10 rings. So if we want to measure at liquid helium temperature, it might be necessary to remove the G10 rings.

A 10 Watt heater should be more than enough to cover the complete temperature range from 10-325 Kelvin (with G10 rings). The temperature range of 2-160 Kelvin appeared to be accessible by replacing the G10 rings with their copper cousins. Preliminary experiments with the copper rings show that the thermal resistance 4.2 Kelvin of the center-unit is at least a factor 10 larger than the number mentioned in Fig. 5.1.

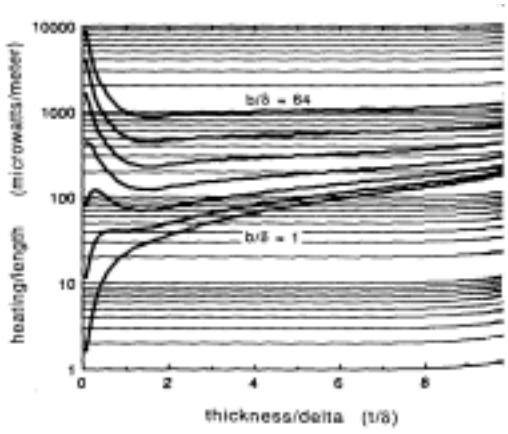

Figure 5.2: Eddy current heating: plots of the expected eddy current heating in microwatts per meter for infinitely long cylinders of radius b, thickness t, and resistivity $\rho = 7 \times 10^{-10}$ Ω-m. The cylinder sits in an axial

Except for above mentioned heat sources there is the parasitic eddy current heating in the copper stage. Because of the ripple of the power supplies (8 ppm), eddy currents are generated. In those materials which have a low electrical resistivity these eddy currents can cause a considerable amount of heat. The graph of Fig. 5.2 shows the heat generated in a hollow cylinder with a wall thickness t and an inner radius b. The cylinder sits in an axial sinusoidal field with an amplitude of 1 Gauss (the ripple of the NHMFL magnets is considerable lower). The skin depth, δ, depends on the electrical resistivity and frequency of the field ripple. For copper it is at 1000 Hz approximately 0.42 mm [24]. From Fig. 5.2 it may be concluded that the eddy current heating in our copper sample stage would be in the μWatt range and can be neglected compared to the laser power.

5.2 Specific heat and helium boil off.

The specific heat of any material is defined from thermodynamics as:

$$C_m = \frac{du}{dT} / m$$

Where u is the internal energy, T is the absolute temperature, and m is the mass of the object.

A summary of the specific heat of the used materials is given in Table 3. The differences are much smaller than those of the thermal conductivity. Note that the values are given per unit mass. The difference per unit volume are even smaller.

Table 3: Specific heat of materials used in the probe (all in call/g.K) [23]

Material	Specific heat at 300 K	Specific heat at 20 K
Copper	0.092	0.0019
Aluminum	0.22	0.0024
stainless steel 18-8	0.11	0.0011
Teflon (close to G10)	0.25	0.018

From the table above we may conclude that the liquid nitrogen and liquid helium necessary for the cool-down procedure can be estimated from the mass of the probe and the vacuum jacket.
After the probe has cooled down and a kind of thermal equilibrium is established, the boil off rate is mainly determined by the cryostat and the vacuum can. A rough estimation by assuming a linear temperature distribution (30K/inch) from the liquid helium level (=4K) to the Quik-fitting at the top to the cryostat (=300K) predicts a helium boil off around 1.5 liter/hour.

5.3 Thermal expansion and contraction.

Most of the materials contract when cooling down. The rate of contraction depends on temperature and material properties. The cummulative unit thermal expansion, $\Delta L/L(T)$, is defined as the total relative expansion $\Delta L/L$, when heating the material up from 0K to the temperature T. Table 4 gives an overview of this parameter for several materials and temperatures.

Table 4: Cumulative unit thermal expansion, $\Delta L/L$ (all in 10^{-5}) [23].

Temp. [K]	Stainless	Alum.	brass	copper	Teflon (G10)
0	0	0	0	0	0
60	4	9	16	12	140
120	49	71	85	67	380
180	122	175	180	149	740
240	208	339	320	273	1450
300	304	418	397	337	1600

The difference in thermal contraction between the G10 and the brass screws with which the G10 rings are tightened is 2/1000 of an inch. This elasticity of the screws should compensate for this.
Because the vacuum jacket is in direct contact with the liquid helium bath, its temperature can be considered to be equal to that of the liquid helium. Although constrictor and center unit will have a temperature close to that of the liquid helium, the rest of the probe will have a much higher temperature. This temperature difference will cause differential contraction and expansion of several parts of the probe during cooling down and heating up. When cooling down the vacuum jacket can shrink 2 mm more than the probe. To avoid that large strains will be built up in the probe, the center unit of MOK3 is spring driven (see also section about the rigidity of the probe).

6. Manipulation rods and sample-stage.

6.1 Realization

For the sample-stage we started of with a vacuum compatible tilting stage of New Focus: the smallest commercially available stage made of stainless steel. A nice stage (6-80 thread tilting screws, $125.- etc.) but slightly magnetic. The two springs (302 stainless steel) and the stainless steel bar that holds them are rather magnetic. Special copper-beryllium springs were ordered via Mcmaster Carr (custom made) (5 springs $120.-). The springs were too weak. After an half year trouble, the stage was set aside for an own design. This is recommendable for everyone who wants to use direct-optics in the long bores of the high field magnets. Starting points are the available springs (non magnetic material: i.e. bronze, copper-beryllium, phosphor-bronze, +/- 10-20 pounds/inch, they can be ordered or they can be home made: McMaster Carr has a spring tool for $80.-).
The tilting stage was designed with the maximum amount of spring power (limited by available space and available springs).. This guaranteed enough rigidity, even with all kind of adapters mounted to the sample table.
The tilting is done by set-screws of normal thread. Both set-screws and stage are made of copper. In order to guarantee low temperature behavior it is furthermore necessary to make the “screw-connection” loose. No low temperature or vacuum lubrication should be used. To be sure that the set-screws will not lock up, it is necessary to have a good vacuum of at least 10^{-2} mbar.
The manipulation rods are stainless steel tubes (0.125” OD) in the higher part, and solid rods (0.1” OD) in the lower part of the lower course of the probe. The tube is closed from the top (atmospheric pressure) and contains a pumping hole in the vacuum can. The

connection between the manipulation rods and the set-screws is via phosphor-bronze allen wrenches which are soldered on the set-screws. A brass hexagonal (2 cm) (McMaster Carr) at the end of the manipulation rods slides over the allen wrenches. The coupling is strong enough to be operated at low temperatures. The slide character of the coupling avoids any differential contraction/expansion problems when measuring at low temperatures. Furthermore it makes disassembling of the sample stage possible.
In the first design a lot of attention was paid on the position and angle of the manipulation rods. From experience we know now that the manipulation rods will still work if they are slightly bent (1-2 cm curve over 2 meter is no problem).

6.2 Adapters.

The sample-stage has been developed so that later all kind of sample holders can be attached to it. Above the sample table there is approximately 0.8”x1” space available. Polar Kerr measurements can be done directly on the sample table (see Fig. 6.1.a). Note that the sample clip is tapered (30 degrees). So or the light reflects with the sample, and the reflected beam find its way back through the vacuum window, or the beam reflects with the slope of the clip and will extinct by multiple reflections in the lower part of the probe.
A heating coil is wounded around the leg of the table. The coil consists of a twisted 32 Maganin wire of 50 ohm. It is taken double to assure that the coil has a zero induction. The connection to the connector on the top is done by a 32 copper twisted pair. Their low resistance guarantees that most of the energy is dissipated in the heating coil. The good electrical conductivity however is accompanied by good thermal conductivity. The copper leads will act as a thermal leak which will become important for the milliKelvin range.
A cernox sensor is mounted in the table just under the sample-platform. Its four contacts are connected to the connector on top of the vacuum window shield by 36 (or 38) phosphor Bronze wires (resistance 65 ohm). As the currents through the sensor are much smaller than those of the heater, thinner wires are sufficient. All leads need to be twisted pairs in order to avoid inductive coupling with the large magnet.
Other adapters have been designed but are not realized yet. Figure 6.1.b.shows an adapter to do Faraday experiments on transparent thin films. If one replaces the sample by a optic cell of Hellma Cell Inc., it is even possible to do Faraday measurements on liquids. Figure 6.1.c shows an adapter for longitudinal measurements. Mirrors are used to get the beam to and from the sample. It should be mentioned here that the effects of those extra two mirrors should be taken in consideration when one is interested in the absolute values

of the MO properties. Furthermore for some angles and material combinations, it is possible that these mirrors corrupt the linear relation between the magnetization and the observed rotations [15]. The results should be interpreted cautiously.

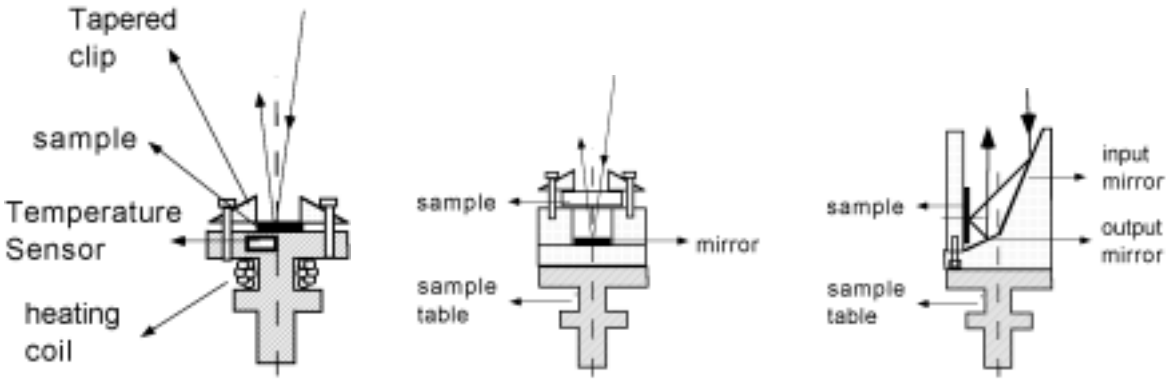

Figure 6.1: (a) polar Kerr holder, (b) polar Faraday holder, (c) longitudinal Kerr holder.

Acknowledgment.

Many people have contributed to the work presented in this report, for which I would like to thank them all. In particular I would like to express my gratitude to a couple of people.
Firstly I would like to thank Prof. Camy Abernathy, Prof. Jeff Childress, and Prof. Steve Pearton for the excellent coaching during my two year stay at the University of Florida in Gainesville. In the last phase of the project their job was taken over by Bruce Brandt, director of operations at the NHMFL facility in Tallahassee. I want to thank him for giving me the opportunity to come to Tallahassee and for the wide support he created for the project.

I owe a great debt of gratitude to Prof. Mark Meissel of the MicroKelvin lab. His advice and references appeared to be of crucial importance to the success of the project. Many other people in Gainesville have to be thanked of whom I would like to mention: Prof Fred Sharifi (vacuum test equipment), Prof. Rolf Hummel (lab space), Prof. John Ziegret (mechanical properties). Prof. Fereshteh Ebrahami and Dan (annealing of the stainless

steel parts), Prof. John Graybeal (material choice), Bob, Bill, Mark, Ed, and Ted (machine shop), Yifeng Yang (low field tests) and last but not least our first lady, Paula (purchase). For the last three months of the project I moved to Tallahassee in order to develop the probe into a user-facility. I'm very much indebted to Vaughn Williams for designing and constructing new manipulation rods, spring driven center unit, and constrictor.
Furthermore I would like to thank Thomas Schmiedel (scientific support), Bobby-Jo (storage box), Nick Pytel (probe holder), Prof. David Lind and D. Kumar (pilot run), Plamen Stoyanov (scientific support), Mark, Dough, Richard & Andy (machine shop), Kevin & John (cryogenics), Mike, Bryon, Shean, Ron & Tina (control room), Scott Hannahs (data acquisition), Cristian Wolters and Erik Palmer (manipulation rods), Stan Tozer (solvent for vacuum grease), and last but not least YongJie Wang (proof reading of this manuscript & cryogenic advice).
Beside the staff of UFL and NHMFL, I also consulted several external experts. I want to acknowledge William van Drent of the University of Twente (The Netherlands) for discussing on several aspects of the measurement technique, William Grifitz of Advance Magnetic Inc. for discussing on the magnetic shielding, and Bob Wang of Hinds Inc. for references and technical support.
Last of all I would like to thank Dieter Weller of IBM in Almaden, and Toshikazu Katayama of the Electrotechnical Laboratory in Tsukuba (Japan) for sending samples. I hope that their initial interest will be followed by many others to come.

References:

[1] F. Rudolf Kessler and Jurgen Metzdorf, "Interband effects and Faraday Rotation", in Landau Level Spectroscopy, vol. 27 of Modern Problems in condensed matter Sciences, G. Landwehr, E.I. Rashba, pp. 579 (1991).
[2] J. Metzdorf, "Linear und Zirkular- Polarisationsmodulation zur Messung der komplexen Magnetorotation. I Messprinzip und Aufbau", Optik 65 (1983) 103-113 (in the German language).
[3] Noboru Miura and Hiroyuki Nojiri, "Low dimensional systems of semiconductors and magnetic materials in very high magnetic fields up to 500 Tesla", Megagauss conference Tallahassee (1995), pp. 684.
[4] H.J. Richter, K.A. Hempel, and J. Pfeiffer, Improvement of sensitivity of the vibrating reed magnetometer, Rev. Sci. Instrum. 59 (1988) 1388.
[5] F. Bitter, Rev. Sci. Instr. 7 (1936) 482.
[6] F. Bitter, "The National Magnet Laboratory at the Massachusetts Institute of Technology.", J. Appl. Phys. 14 (1963) 759-765.

[7] J. E. Crow, D. M. Parkin, H. -J. Schneider-Muntau, and N.S. Sullivan, “The National High Magnetic Field Laboratory: An Introduction to Science and Technology Opportunities.”, Proceedings of the Megagauss conference in Tallahassee (1995) 1-15.
[8] NHMFL year report 1995-96.
[9] William van Drent, PhD. Thesis University of Twente, The Netherlands (1995).
[10] Wim Geerts, PhD. Thesis University of Twente, The Netherlands (1991), Magnetization distribution at the surface of sputtered Co-Cr films: structural, chemical, and magneto-optical characterization.
[11] private communication with Dr. Plamen Stoyanov.
[12] Y. Suzuki, T. Katayama, W. Geerts, Symp. Mat. Res. Soc.
[13] Private communications with application engineer of Melles Griot.
[14] Katsuaki Sato, Measurement of magneto-optical Kerr effect using piezo-birefringent modulator, Jap. J. Appl. Phys. 20 (1981) 2403-2409.
[15] W.J.M.A. Geerts, et al. Rev. Sci. Instrum.63 (1992) 1805-1809, forgive me the sign errors in this paper.
[16] Bas Zeper, PhD. Thesis University of Twente, The Netherlands (1992).
[17] A. Mager, “Das Eindringen von Magnetfeldern in offene Abschirmzylinder”, Z. Angew. Phys. 23 Bd., Heft 6 (1967) 381-386.
[18] Albrecht J. Mager, “Magnetic Shields”, IEEE Trans. on Magn., Mag-6 (1970) 67-75.
[19] A complete guide to Magnetic Shielding, publication of Amuneal Manufacturing corporation, phone: 215-535-3000, fax: 215-743-1715.
[20] Bozorth 146-153.
[21] Bob of the machine-shop in Gainesville.
[22] Roy R. Craig Jr., Mechanics of Materials, John Wiley & Sons, New York 1996
[23] Klaus D. Timmerhaus and Thomas M. Flynn, Cryogenic Process Engineering”, 1989 New York.
[24] Eric S. Meyer and Isaac F. Silvera Lyman, Bruce L. Brandt, “Eddy current shielding and heating: reduction of dissipation for very low temperature experiments in the presence of magnetic field ripple, RSI, 60: 2964-2968 (1989).
[25] F. Bitter, “Water Cooled Magnets”, Rev. Sc. Instrum. 33 (1962) 342-349.
[26] Frank L. Pedrott, Leno S. Pedrotti, Introduction to optics, Prentice Hall, New Jersey, 1987.
[27] Handbook of Chemistry and Physics.

Addresses and Telephone numbers.

Advance Magnetics Inc.
Magnetic Shielding
Application engineer: William Grifitz
Marketing: Kay Nixon
625 Monroe Street, P.O. Box 69, Rochester, Indiana 46975
phone: 219-223-3158 fax: 219-223-2524

Amuneal Manufacturing corp.
Marla J. Lantz.
Magnetic shielding
4737 Darrah St. Philadelphia, PA. 19124.
phone: 215-535-3000 fax: 215-743-1715

Scientific Alloys Inc.
supplier of the shields of Magnetic iron
P.O. Box 523, Westerly, R.I. 02891
Jim Rossi
phone: 401-596-4947 fax: 401-596-4947

Hinds Instruments
PEM modulator and signal conditioner
Dr. Bob Wang
3175 NW Aloclek Drive, Hillsboro, OR 97124-7135
phone: 503-690-2000

Gsanger Optoelektronik GmbH
Frank Reissmann
electrooptical modulators.
Robert-Koch Strasse 1a, D-82152 Planegg / Germany
tel: 089-859-5621 fax: 089 - 859-7875

Conoptics Inc.
Ronald J. Pizzo
Electro-Optical modulators.
19 Eagle Road, Danbury, CT. 06810

Phone: 203-743-3349 Fax: 203-790-6145
e-mail: conoptic@aol.com

Goddard valve corp.
Leon Schriber
Quik-fittings.
P.O. Box 765, Worcester, MA 01613
phone: 508-852-2435 fax: 508-852-2443

McMaster Carr
general supplies: springs, screws, tubes, raw materials, wires, phosphor bronze allen wrenches, bronze hexagonals. etc.
P.O. Box 740100 Atlanta
GA 30374-0100
phone: 404-346-7000 fax: 404-349-9091

Melles Griot
general optics
Bob Valdez
1770 Kettering Street
Irvine, CA 92714
phone: 714-261-5600 fax: 714-261-7589

Karl Lambrecht Corp.
polarizers in the far UV
Vino
fax: 773-472-2724

Thorlabs Inc.
P.O. Box 366
Newton NJ 07860-0366 USA
phone: 201-579-7227 fax: 701-383-8406
e-mail: www.thorlabs.com

Florida Offshore supply Inc.
stainless steel tube with an OD of 1 3/8”
Jeff Walker (gator fan)
587 Northride trail, FL33813 Lakeland

phone: 941-648-4501 fax: 941-644-3385

New Focus Inc.
Tilting stage MOK1, + non-magnetic tilting stage for alignment incident beam.
Khiem Do
2630 Walsh Avenue, Santa Clara, California 95051-0905
fax: 408-980-8883

Economy spring and stamping company
John Wisyanski: supplier of springs for New Focus mount (only large quantities)
29 DePaolo Drive, P.O. Box 651, Southington, CT 06489
tel: 860-621-7358 fax: 860-621-7882

Marco Springs
Norman Marik
Custom design spring, fast delivery, no non-magnetic materials.
1187 Severson Ave., Memphis, Tennessee 38106
phone: 901-942-7272 fax: 901-942-7273

Associated Spring
Scott Frommer, stock springs
18 Main Street, Bristol, CT 06010
tel: 203-582-9581

Century Springs
stock springs, catalogue at NHMFL ask Vaughn William
222 East 16 Str. , Los Angelos CA 90015
phone: 213-749-1466 fax: 213-749-3802

Hellma cells
David Friedmann
Cells for Faraday measurements on liquids.
Phone: 718-544-9534 fax: 718-263-6910

List of Figures: